Geomechanics and Engineering, *Vol. 41, No. 1 (2025) 71-82*
https://doi.org/10.12989/gae.2025.41.1.071

Compressional behavior of fine-grained soils: Clastic and biogenic silty soils

Handikajati K. Marjadi[a] and Junbong Jang*

Department of ICT Integrated Ocean Smart Cities Engineering, Dong-A University, Nakdong-daero 550beon-gil, Saha-gu, Busan 49315, Republic of Korea

(*Received November 22, 2024, Revised February 22, 2025, Accepted March 5, 2025*)

Abstract. Infrastructure construction on coastal areas such as ports, bridges and airports require ground improvements when marine soils contain soft ground which includes fine grains in general. Fine-grained soils consist of clastic or non-clastic grains. Based on the mineralogy of soils, compressibility of soils shows different behavior. Fine-grained clay mineral soils show plastic and time-dependent deformation due to consolidation during constructions while silty soils without clay minerals show low compressibility. However, biogenic soils such as diatomaceous earth are more compressible than other silty fine-grained soils. Although fine-grained soils with clastic minerals and biogenic minerals are classified as silt, the behavior of clastic soils are less compressible compared to biogenic soils which have inner pores. We conducted one-dimensional consolidation experiments to investigate compressibility of diatomaceous earth and non-plastic mineral fines such as silica silt. The coefficient of consolidation, and volumetric compressibility are estimated, and show that the trends of diatomaceous earth properties are different from other silty soil properties based on the consolidation tests. We found that particle breakage plays a crucial role in compressibility of diatomaceous soils. While the compressibility of diatomaceous soils is similar to clastic soils at low stress, the differences in compressional behavior between two soils are distinct at high stress. The diatomaceous earth shows time-dependent compressibility due to creep or secondary compression by particle breakage process. Thus, settlement analysis should include the impact of morphology and mineralogy of fine-grained soils.

Keywords: compressibility; diatomaceous earth; mineralogy; secondary compression; silty soil

1. Introduction

Fine-grained soils with clay minerals would be problematic due to high compressibility when structure loads on the ground are applied. Soft ground is a major constraint on development in coastal areas, due to its low strength, low permeability, and high compressibility (Li *et al.* 2023). For stable construction, the soft ground should be improved by controlling the compressibility (Han 2015), for example, by accelerating the rate of consolidation, or reinforced by supporting structure such as sheet pile (Aparna and Bindu 2023, Nguyen *et al*. 2023). In case of compressibility control, time-dependent settlement analysis is essential to calculate settlements and construction costs for ground improvement. Terzaghi's consolidation theory is a fundamental settlement analysis to 1D consolidation lab tests (ASTM D2435 2011, Taylor 1948). For field observation, Asaoka method, hyperbolic method, and Hoshino method can be used (Asaoka 1978, Li *et al.* 2024, Sridharan and Rao 1981, Tan and Chew 1996,). Both lab and field settlement assessment help geotechnical engineers decide total settlement and settlement time.

Many researchers studied various factors that are relevant to soil structure can affect the soil compressibility (Al-Shamrani 2005, Li 2014, Zhang *et al.* 2014). First, the origin of sedimentation is one of compressibility factors. Soft grounds with fines can form naturally or artificially. Fine-grained soils naturally deposit at low-energy environments such as offshore areas (Nichols 2009). When fine-grained sediments at coastal area are dredged and filled, the artificially reclaimed areas with the fines become soft grounds without diagenetic effects of soils such as cementation. Sedimentation environment would determine the initial soil structure that would affect the compressional behavior of reclaimed areas and natural soils.

The soil compressibility is dependent on physical properties of soil particles. The large specific surface area of individual fine particles allows it to adsorb pore water onto particle surfaces resulting in high water content and settlement (Kwon *et al*. 2019). The ability of a particle to adsorb water is influenced by its mineralogical composition (Lambe and Whitman 1969, Santamarina *et al.* 2001). Predominant minerals of marine soils are quartz, feldspar, and clay minerals (Brydon and Patry 1961, Hyodo *et al.* 2017, Scarciglia *et al.* 2006) and the minerals are from clastic and non-clastic or biogenic processes. Clastic particles form based on crystal growth while the non-clastic or biogenic particles are from microorganisms that generate inner pores and complex shapes.

Diatomaceous earth among biogenic particles are the fossilized frustule or skeletons of diatoms (Cho *et al.* 2017, Shiwakoti *et al.* 2002, Jang *et al*. 2022). Diatoms absorb

*Corresponding author, Associate Professor
E-mail: jjang@dau.ac.kr
[a]Ph.D. Student

ISSN: 2005-307X (Print), 2092-6219 (Online)

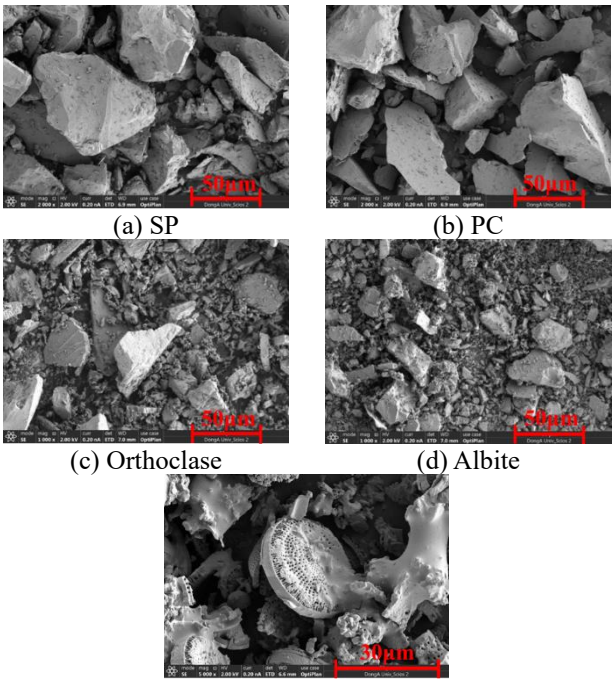

(a) SP (b) PC (c) Orthoclase (d) Albite (e) Diatomaceous Earth - DE

Fig. 1 Scanning electron microscope (SEM) images of silty soils: (a) Finer silica silt (SP), (b) Coarser silica silt (PC), (c) Orthoclase, (d) Albite and (e) Diatomaceous Earth (DE)

Table 1 XRD analysis of mineralogical content in each soil

No	Soil Type	Mineralogical Content
1	Diatomaceous Earth - DE	Cristobalite: 96.6%; Quartz: 3.4%
2	Silica Silt - SP	Quartz: 80.1%; Muscovite: 19.9%
3	Silica Silt - PC	Quartz: 95.8%; Muscovite: 4.2%
4	Orthoclase	Orthoclase: 72.8%; Albite: 24.2%; Muscovite: 3%
5	Albite	Albite: 83.5%; Quartz: 13.9%; Muscovite: 2.6%

dissolved silica from water and create rigid cell walls that provide both protection and structural support. When the diatoms die, these cell walls settle and accumulate as sedimentary deposits. Diatomaceous earth particles are composed of an amorphous silica structure characterized by an irregular skeletal texture, leading to a low specific gravity and inner porosity (Pedone *et al.* 2022). As the content of diatomaceous earth increases, the specific gravity of the soil mass correspondingly decreases. Particle sizes range from 20 µm to 2 mm, and the various particle shapes include internal porosity that can hold pore fluid (Zuluaga-Astudillo *et al.* 2022).

The morphology of the diatomaceous earth shows high effective friction angle and shear strength due to the high angularity of the particle (Karabash and Cabalar 2023) along with high liquid limit and non-plastic behavior (Khraisheh *et al.* 2005, Shiwakoti *et al.* 2002). Diatomaceous earth is classified as elastic silt (MH) based on the unified soil classification system (USCS) (Perisic *et al.* 2019, Zuluaga-Astudillo *et al.* 2022) unlike clastic silty soils (Tiwari and Ajmera 2011). Because of the morphology, diatomaceous earth frequently exhibits high compression index (C_c), primarily caused by the susceptibility of its particles to breakage. Therefore, diatomaceous earth is generally more compressible than clastic-rich silty sediment (Jang and Marjadi 2023). The *e*-log$(\sigma`_v)$ curve characteristics of reconstituted diatomaceous earth is concave downward, denoting yield stress around 200 kPa (Shiwakoti *et al.* 2002), in another case of 540 kPa (Perisic *et al*. 2019). The inherent fragility of these particles stems from their amorphous silica structure, which is weaker under pressure than its crystalline counterparts (Pedone *et al*. 2008). Upon compression of sand-diatomaceous earth mixture, the content of fine particles increases when the mixtures are subjected to a specific loading pressure which is inferred to particle breakage pressure (Hoang *et al*. 2022). Compression index of kaolin-diatomaceous earth mixture also increases as the proportion of diatomaceous earth goes up (Díaz-Rodríguez and González-Rodríguez 2013, Sonyok and Bandini 2019). Moreover, compressional mechanism of biogenic fines is unclear compared to that of clastic fines.

This study aims to quantitatively analyze the time-dependent compressional behavior of biogenic silts such as diatomaceous earth compared to clastic silts. 1D incremental loading tests may provide time-dependent compressibility factors that include permeability, coefficient of volume compressibility, and coefficient of consolidation, and secondary compression. Compressibility mechanism of biogenic silts would be evaluated based on the trend of the compressibility factors. We would suggest methods to calculate settlements of biogenic soils and explore how this mechanism affects its compressibility behavior under axial loading.

2. Methodology

2.1 Material properties

We used commercially available silty soils that have different mineralogy: two silts with different median sizes (SP and PC), the potassium feldspar (orthoclase), the sodium feldspar (albite), and diatomaceous earth (DE). Scanning electron microscopy (SEM) provides the morphology of the soils (Fig. 1). The SEM images show that the shapes of quartz (SP and PC) and feldspars (albite and orthoclase) are angular and bulky. In contrast, DE particles are disc-shaped structure with internal pores. X-ray diffraction (XRD) analysis confirms mineral compositions of the soils (Table 1). Diatomaceous earth can be detected using XRD by observing the content of amorphous opal or the opal conversion to cristobalite at high temperature (Shiwakoti *et al.* 2002).

Material characteristics are presented in Table 2. Diatomaceous earth (DE) is classified as MH, while the other materials are categorized as silt (ML) according to the USCS (ASTM 2011a). The particle sizes of the soils are within silt sizes which are measured from hydrometer tests

Table 2 Index properties of silty soils

No	Soil Type	Specific Gravity[(a)], G_s [ ]	Median Particle Size[(b)], D_{50} [μm]	Specific Surface Area[(c);(d)], *SSA* [m²/g]	Plastic Limit[(e)], ω_{PL} [ ]	Liquid Limit[(f)], ω_{LL} [ ]	Plasticity Index, *PI* [ ]	USCS
1	Diatomaceous Earth-DE	2.32	11	1.57[(c)]	157	168	11	MH
2	Silica Silt-SP	2.69	31	0.328[(d)]	30	33	3	ML
3	Silica Silt-PC	2.72	42	0.291[(d)]	29	35	6	ML
4	Orthoclase	2.6	17	0.433[(d)]	27	34	7	ML
5	Albite	2.67	10.5	0.384[(d)]	25	28	3	ML

[(a)]Water Pycnometer (ASTM D854); [(b)]Hydrometer (ASTM D7928); [(c)]Methylene blue spot test (Santamarina et al. 2002); [(d)]Spherical Particle Shape Analysis (Chapuis *et al.* 2003); [(e)]Hand rolling (ASTM D4318); [(f)]Fall cone test (BSI1377 Part 2)

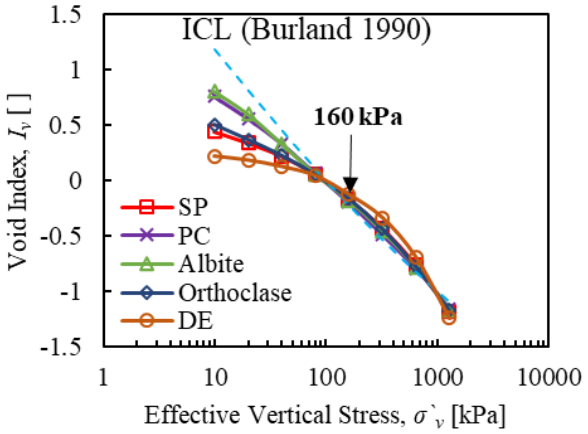

Fig. 2 Normalized compression curves of the materials based on void index and comparison with intrinsic compression line (ICL)

(ASTM 2016). The specific surface area of the bulky particles (SP, PC, albite, and orthoclase) can be estimated from particle size distributions (Chapuis *et al.* 2003). Specific surface area of DE was estimated by the methylene blue spot test (Santamarina *et al.* 2002, Jang *et al*. 2018). DE has a low specific gravity, high liquid limit (ω_{LL}) and low plasticity due to the skeletal structure with inner pores.

2.2 Consolidation test

One-dimensional consolidation tests based on ASTMD2435 (ASTM 2011b) were conducted to characterize the compressional behavior of the soils. First, each material was prepared by mixing with deionized water at $1.25\omega_{LL}$ (Burland 1990). After saturating the sample in 12 hours, each sample was transferred into a consolidation ring which has 2 cm in height and 6 cm in diameter. Subsequently, the oedometer was set up and placed on the loading frame. The liquid reservoir of the oedometer was filled with deionized water. The seating load of 5 kPa for 12 hours was applied. Then, the sample was subjected to a series of loading stages with increment ratio (IR) of 2 until 1280 kPa is reached. The duration of each loading step is 24 hours. A series of unloading stages with 1/4 of IR up to 10 kPa was followed and reloading stages were applied. The vertical deformation was automatically recorded by digital device (Mitutoyo 543-260, 1μm precision) and GEOTM consolidation software.

3. Results

3.1 Stress-strain characteristics

The compressibility of silty soils is influenced by the initial conditions prior to the loading steps such as water content and pore water salinity (Georgiannou *et al.* 2018). We normalized the consolidation results with the void index, I_v (Burland 1990).

$$I_v = \frac{e - e^*_{100}}{e^*_{100} - e^*_{1000}} \quad (1)$$

where e^*_{100} represents the intrinsic void ratio at 100 kPa, and e^*_{1000} is the intrinsic void ratio at 1,000 kPa. The term "intrinsic" refers to the soil state that has no diagenesis or aging effects in the soil structure at a water content between $1.2\omega_{LL}$ and $1.5\omega_{LL}$ times to liquid limit water content where the natural in-situ state would make minimal influence on the mechanical behavior of reconstituted soil. The compression curve follows the intrinsic compression line (ICL).

$$I_v = 2.45 - 1.285\log(\sigma`_v) + 0.015(\log(\sigma`_v))^3 \quad (2)$$

Fig. 2 presents the normalized compression curves of the silty soils we tested. The shapes of the curves are concave downward. The curves deviate from the ICL below 100kPa. The DE curve deviates most from the ICL at low stress levels. The deviation of the compression curves from the ICL line are presented as a third-degree polynomial equation (Wang *et al*. 2022).

$$I_v = D + C\log(\sigma`_v) + B\log(\sigma`_v)^2 + A\log(\sigma`_v)^3 \quad (3)$$

where *A*, *B*, *C*, and *D* represent fitting parameters (Table 3). Parameters *A* and *B* are function of coefficient of uniformity (C_u), which is reversely proportional to C_c (Minh and Cheng 2013). Parameters *C* and *D* are relevant to initial liquidity index (LI_i) which affects the soil state at the beginning of the loading as shown in Fig. 3. However, DE stands out as an outlier in these correlations due to particle breakage occurring under loading steps.

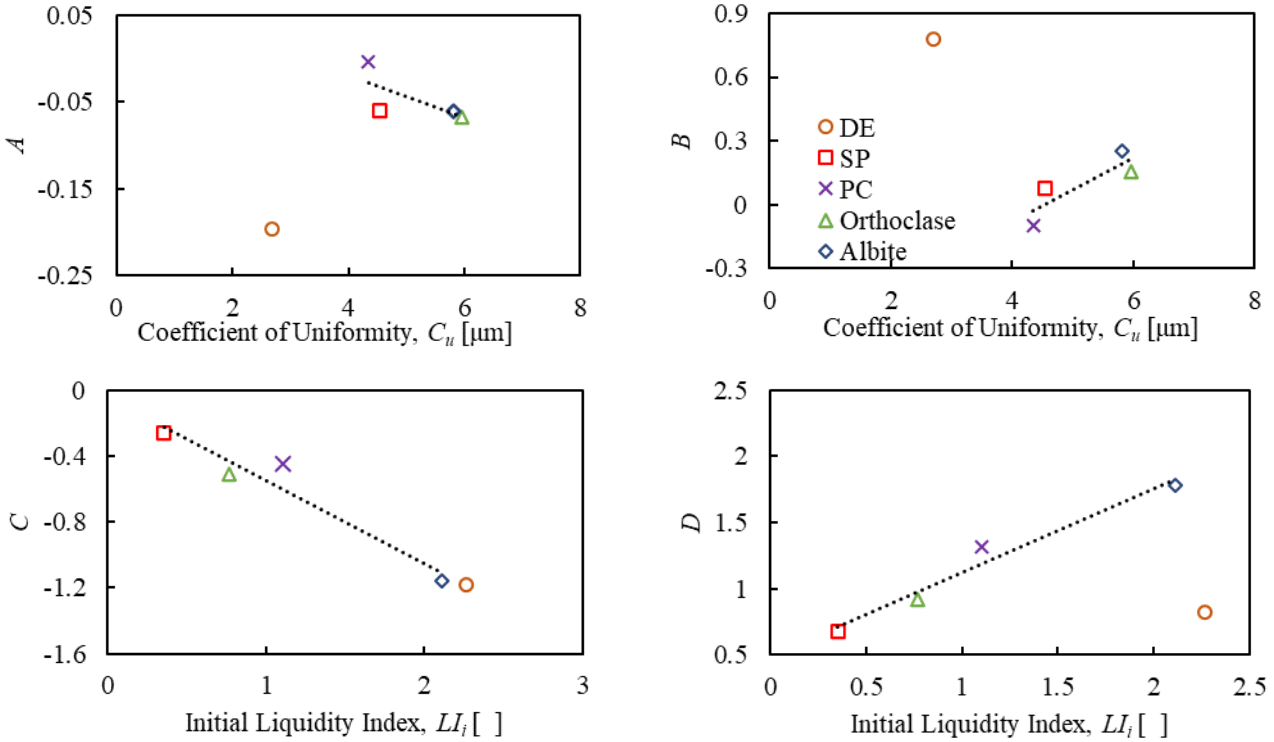

Fig. 3 Correlation between coefficient of uniformity (C_u) with fitting parameter *A* and *B*, and between initial liquidity index (LI_i) with fitting parameter *C* and *D*

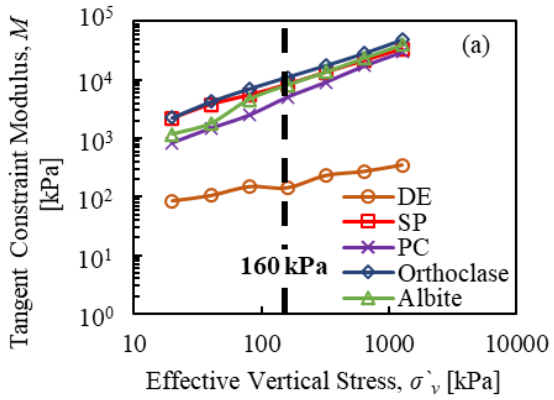

Fig. 4 Variation of tangent constraint modulus (*M*) with effective vertical stress

During the consolidation tests, the vertical stresses are transferred through particles and rearrange the particles. The stress concentration during the stress transfer can induce particle damage or crushing. The damages can be categorized by three levels. Level I is abrasion or grinding of the particle surface, level II the breaking of corners or edges, and level III complete particle crushing or shattering (Mesri and Vardhanabhuti 2009). The particle breakage of soil can be inferred by observing the trend of tangent constraint modulus (*M*) at each vertical stress

$$M = \frac{\Delta\sigma_v^{`}}{\Delta\varepsilon_v} \tag{4}$$

Table 3 Coefficients in void index equation

No	Soil Type	*A*	*B*	*C*	*D*
1	Diatomaceous Earth - DE	-0.197	0.779	-1.178	0.818
2	Silica Silt - SP	-0.06	0.075	-0.256	0.679
3	Silica Silt - PC	-0.004	-0.098	-0.45	1.316
4	Orthoclase	-0.067	0.154	-0.508	0.922
5	Albite	-0.06	0.253	-1.154	1.777

where $\Delta\sigma`_v$ and $\Delta\varepsilon_v$ are the changes in effective vertical stress and vertical strain, respectively. An increase in *M* typically indicates a more pronounced locking effect among particles whereas a decrease in *M* implies dominant unlocking effects, such as particle breakage. Fig. 4 illustrates the trend of *M* during the loading stage, where *M* values for all materials generally increase. The *M* of DE is relatively constant. Specifically, a plateau trend at 160 kPa suggests that a significant unlocking mechanism of level III particle damage may be balanced out by becoming dense packing. The yield stress of diatomaceous earth can be identified at 160 kPa which is the turning point on the bi-linear curve in Fig. 2. This observation indicates that the compressional behavior of DE is different from clastic soils.

Compressibility commonly is quantified by intrinsic compression index (C_c^*) and swelling index (C_s).

$$C_c^* \text{ or } C_s = \frac{e_{100}^* - e_{1000}^*}{\log\left(\frac{1000kPa}{100kPa}\right)} \tag{5}$$

Table 4 Indices of compressional behavior and influential factors

No	Soil Type	Initial Liquidity Index, LI_i [ ]	Coefficient of Uniformity, C_u [ ]	Intrinsic Compression Index, C_c^* [ ]	Swelling Index, C_s [ ]	C_c^*/C_s [ ]
1	Diatomaceous Earth-DE	2.267	2.7	0.159[(a)]; 1.072[(b)]	0.101	10.656[(b)]
2	Silica Silt-SP	0.354	4.5	0.078	0.023	3.602
3	Silica Silt-PC	1.106	4.4	0.117	0.020	5.730
4	Orthoclase	0.770	6.0	0.063	0.019	2.524
5	Albite	1.129	5.8	0.079	0.018	2.807

[(a)]Slope of compression curve below 160 kPa. [(b)]Slope of compression curve above 160 kPa

On a reconstituted sample, these indices are calculated from Eq. (5) and are presented in Table 4. We calculated C_c^* of DE in two slopes of the curve below 160 kPa and above 160 kPa, and C_s of DE is calculated from Eq. (5). Table 4 indicates that higher C_u corresponds to lower C_c^*. Within the same mineralogy, the effect of LI_i is more relevant to C_c^*. The soils with higher LI_i have higher C_c^*. Compared to other soils, C_c^*/C_s ratio of DE is significantly higher, indicating substantial plastic deformation.

3.2 Evolution of k, m_v, and c_v

DE has significant compressibility compared to the clastic silts (Fig. 5(a)). The void ratio changes are relevant to the permeability. Fig. 5(b) shows the evolution of hydraulic conductivity (k) as the vertical stress increases. The permeability of non-cohesive soils can be estimated using the empirical equation for various soil types (Chapuis *et al*. 2003):

$$\log(k) = T + \log\left(\frac{e^3}{Gs^2\, SSA^2\, (1+e)}\right) \tag{6}$$

The T is a constant for the tortuosity and shape of flow channels, and we used T=0.5. Eq. (6) was employed to estimate the hydraulic conductivity of the soils during consolidation tests. The soils with larger particles exhibit higher hydraulic conductivity, except for DE. Despite its relatively small particle size, DE demonstrates high hydraulic conductivity due to its particle shape, which includes a large volume of internal porosity and rough surfaces. Consequently, the presence of diatomaceous earth in soil influences the overall soil hydraulic conductivity (Shiwakoti *et al*. 2002). The decrease in hydraulic conductivity for DE is more pronounced compared to other clastic soils under higher stresses. Abrupt change in hydraulic conductivity variation is observed in DE, in contrast to the other soils which show a linear decrease on a logarithmic scale. Pore fluid primarily flows through interparticle void channels which have less surface area and therefore less resistance to fluid flow (Johnson *et al*. 2003). When extensive particle breakage occurs, inner voids are exposed, allowing fluid to flow through more smaller channels and over a larger surface area, resulting in a significant decrease in hydraulic conductivity.

Fig. 5(c) indicates that particle breakage occurred in DE by comparing variations in the coefficient of volume compressibility (m_v)

$$m_v = \frac{e}{(1+e)\,\Delta\sigma_v`} \tag{7}$$

At the same stresses, DE shows moderate m_v at lower stresses but the highest m_v at higher stresses among the soils. We infer that the compressibility of DE with the particle breakage increases due to unlocking mechanism. Fig. 5(d) shows the evolution of coefficient of consolidation (c_v) with vertical effective stresses. The graphical methods such as the Casagrande method were improper to obtain c_v for silty soils. The coefficient of consolidation can be calculated from the Terzaghi's consolidation theory

$$c_v = \frac{k}{m_v\, \gamma_w} \tag{8}$$

where γ_w is the unit weight of pore fluid. While k and m_v generally decrease as $\sigma`_v$ increases, leading to an expected constant variation in $c_v$, several studies have demonstrated that $c_v$ can either increase or decrease with increasing $\sigma`_v$ (Bohnhoff and Shackelford 2014, Robinson and Allam 1998). The variation in c_v of clastic silty soils is proportional to the effective vertical stress primarily due to mechanical compressibility mechanisms (Robinson and Allam 1998). However, the c_v of DE behaves differently as c_v increases at lower stresses and decreases at higher stresses. In case of DE, the particle breakage at high stress causes particle rearrangement and inner pores exposed. As the k decreases through narrow flow channels, c_v goes down accordingly.

The compressibility-related parameters of diatomaceous earth would deviate from empirical correlations and models for the compressibility of clastic soils because of the bi-linear behavior with stress in Fig. 5. Engineers need to include these nonlinear behaviors when designing foundations, embankments, or infrastructure on diatomaceous earth-rich sediments. The use of stress-dependent behavior is essential when evaluating the long-term stability and consolidation behavior of diatomaceous earth.

3.3 Secondary compression

The secondary compression can critically affect the long-term serviceability of structures (Ng *et al*. 2013,

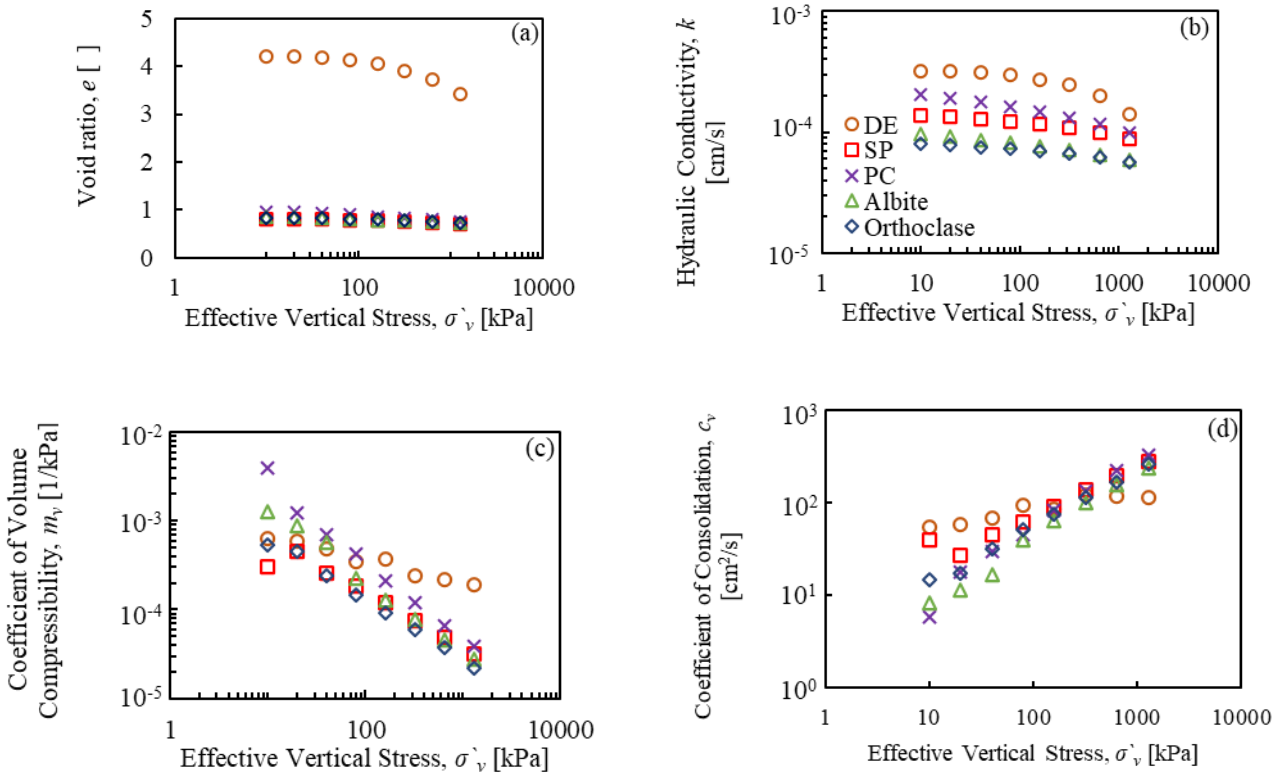

Fig. 5 Compressibility parameters with the effective vertical stress by the consolidation results of non-plastic soils: (a) *e*-log($\sigma`_v$) curve, (b) hydraulic conductivity (k), (c) coefficient of volume permeability (m_v), and (d) coefficient of consolidation (c_v)

Sobhan *et al.* 2012, Stark *et al*. 2005). The secondary compression index (C_α) for the secondary compression settlement can be obtained at the straight-line portion of *e*-log(*t*) curve

$$C_\alpha = \frac{\Delta e}{\Delta \log t} \tag{9}$$

Fig. 6 highlights the long-term compressibility of DE compared to the other clastic soils. DE has comparably higher C_α, while the other soils show similar values. Thus, C_α increases with increasing diatomaceous earth content (Sonyok and Bandini 2019). The secondary compression of DE is influenced by the particle breakage and particle rearrangement. When the load initiates particle breakage, the void ratio declines, the relative density rises, and the contact force reduces (Chang and Deng 2020, Li *et al*. 2023, Xiao *et al*. 2017), which leads to the significant particle rearrangement induces the secondary compression. Fig. 7 illustrates the comparison of time-dependent compressional behavior among the soils and the impact of particle breakage on the long-term axial deformation of DE. The y-axis is the normalized void ratio from 0 to 1 which the void ratio at the beginning of a loading stage is unity. and that at the end of the stage is zero. Below 160 kPa, the curves of all materials are clustered together. Above 160 kPa, the DE curvature increases and moves upward, extending beyond the typical range of other clastic soils.

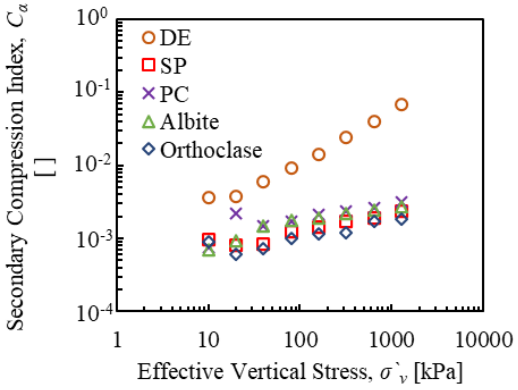

Fig. 6 Change on the secondary compression (C_α) of the silty soils with effective vertical stress

The phenomenon is attributed to both particle breakage and particle rearrangement mechanisms.

The C_α/C_c ratio is determined by the coefficient of the best fit line from C_α-C_c plot (Mesri and Castro 1987) to analyze secondary compression (Mesri and Godlewski 1977). C_c is determined by measuring the slope of *e*-log($\sigma`_v$) at each loading. Fig. 8 shows the C_α/C_c of each soil, and the values of the clastic soils fall within 0.015 ~ 0.03 which is similar to the crushed sand (Mesri and

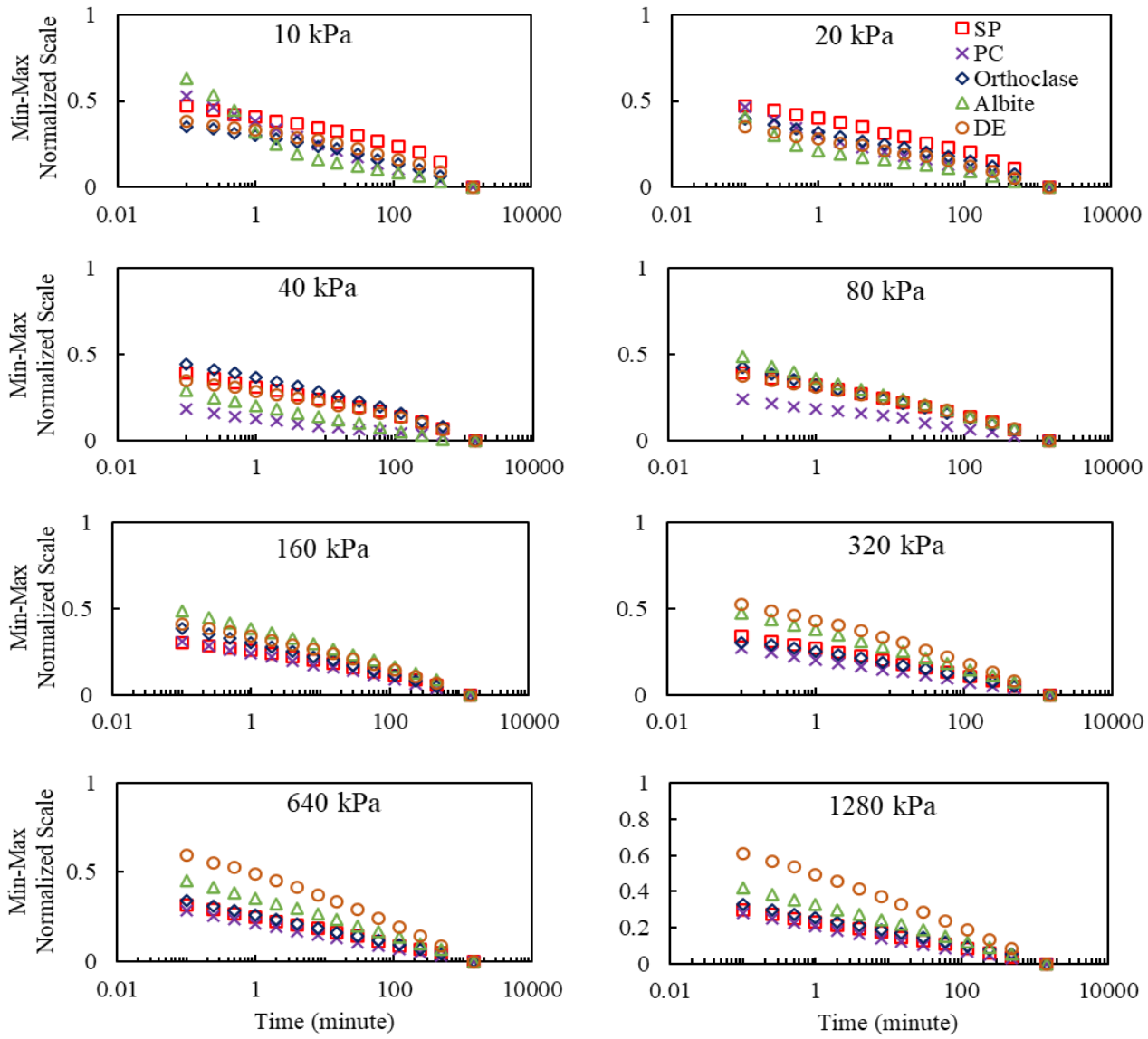

Fig. 7 Normalized axial deformation with time at each loading step

Vardhanabhuti 2009). DE has higher C_α/C_c value of 0.0504 due to particle crushing. Comparable studies on soils with diatomaceous earth also show that C_α/C_c ranges from 0.04 to 0.075 (Mendoza *et al.* 2022, Perisic *et al.* 2019, Sonyok and Bandini 2019).

4. Discussions

4.1 Compressional behavior changes based on stress

The compressibility of clastic silty soils is typically associated with the initial liquidity index and the coefficient of uniformity (Section 3.1). A parametric analysis using multilinear regression was performed with the initial liquidity index and coefficient of uniformity of the clastic soils to estimate the compression index (Table 5), and the results can be expressed as

$$C_c^* = \frac{0.4}{C_u} + 0.0067LI_i \quad (10)$$

The compression index of all materials including DE below 160 kPa where particle breakage is minimal, effective vertical stresses are predicted using Eq. (10). The predicted values are similar with measured values where the plot scatters close to the 1:1 line (Fig. 9). As shown in Table 5, the initial liquidity index of DE is significantly higher compared to other clastic soils. DE also has the lowest coefficient of uniformity. The initial void ratio and coefficient of uniformity induce the highest compressibility below 160 kPa among the soils tested. The compressional behavior of DE, prior to particle crushing, is similar to that of clastic silty soils.

However, when the particle crushing is introduced at the stress over 160 kPa, the compressional behavior of DE is different from that of the clastic silty soils. The particle

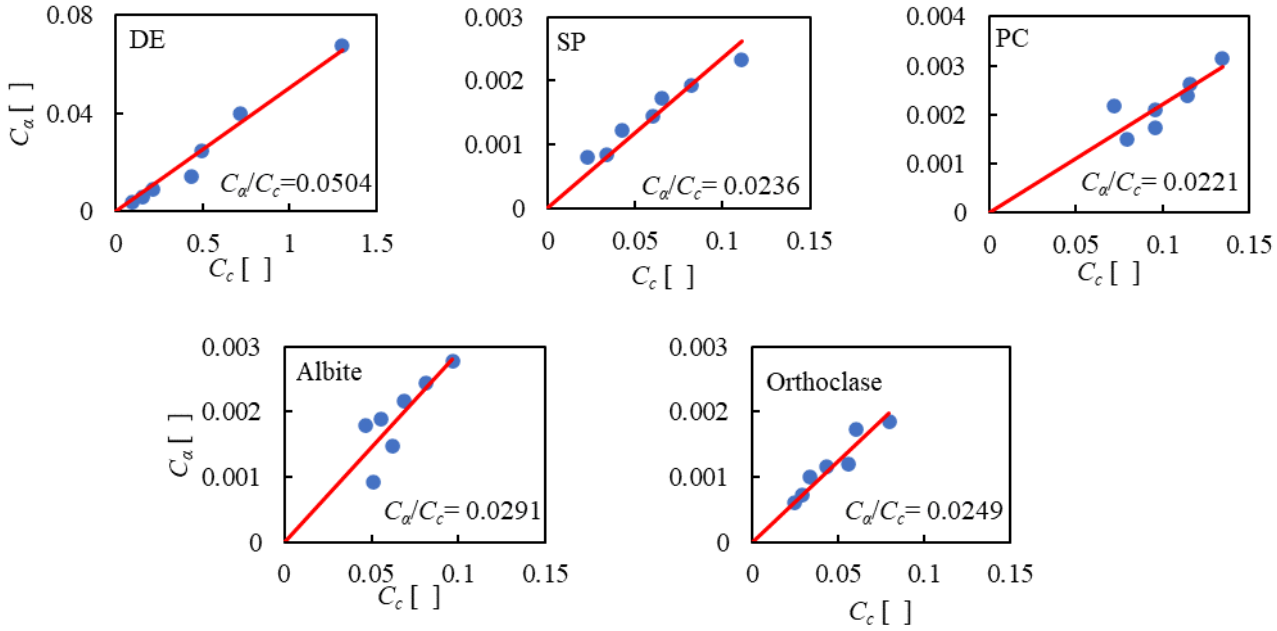

Fig. 8 Evaluation of C_α/C_c ratio of each silty soils. Red line represents the regression line of C_α-C_c plot where the slope of the regression line is the value of C_α/C_c

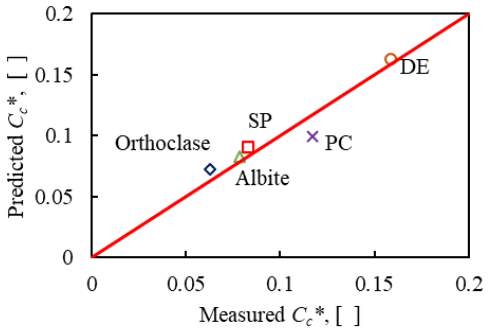

Fig. 9 Predicted and measured compression index (C_c^*). The red line represents the 1:1 line

crushing would produce smaller particles and stress path through the particles and that would alter particle arrangements and size distribution. This alteration would be relevant to the increase in the secondary compression in the long-term deformation and cause misunderstanding of the assessment of geotechnical engineering designs if the settlement calculation is based on clastic soils.

4.2 Implications of diatomaceous earth content on soils

We can find high compressibility of diatomaceous earth in nature. For example, diatomaceous earth sediments near Mejillones Bay in Chile brought higher compressibility compared to those of fine soils as significant creep strain was noted after yield stress, suggesting time-delayed crushing of diatomaceous earth particles (Perisic *et al.* 2019). Biogenic soils in the Ulleung Basin, South Korea,

Table 5 Empirical equation for compression index

c_1	c_2	R^2	Selected Predictors
-	0.0584	0.7089	LI_i
0.435	-	0.9814	$1/C_u$
0.400	0.0067	0.9846	LI_i;$1/C_u$

$C_c = c_1 \times 1/C_u + c_2 \times LI_i$

were studied both the mineralogical composition and compression index of the soil (Jang *et al.* 2022). One notable finding was that the compression index increased with higher diatomaceous earth content although the content of mica and illite decreases. The diatomaceous earth plays the dominant role in controlling the compressibility of the soil.

The compressional behavior of soils is dependent on the particle arrangement and the initial void ratio is critical to the compression index. Accordingly, the compression index of soil mixtures can be anticipated based on the soil content when the mixture consists of clastic soils (Tiwari and Ajmera 2012). When diatomaceous earth is involved, it would affect the compressional behavior. The kaolin-diatomaceous earth mixtures would have the compression curves shift to higher void ratios, and the compression index increases as the diatomaceous earth content increases (Caicedo *et al.* 2019). This occurs because the stress transfer through diatomaceous can induce particle crushing and the secondary compression. Also, the presence of diatomaceous earth can alter the compressional behavior of sand-diatomaceous earth mixtures. The compressibility of sand mixed with diatomaceous earth shows more irrecoverable plastic deformation as the diatomaceous earth content increases (Hoang *et al.* 2022). As the diatomaceous

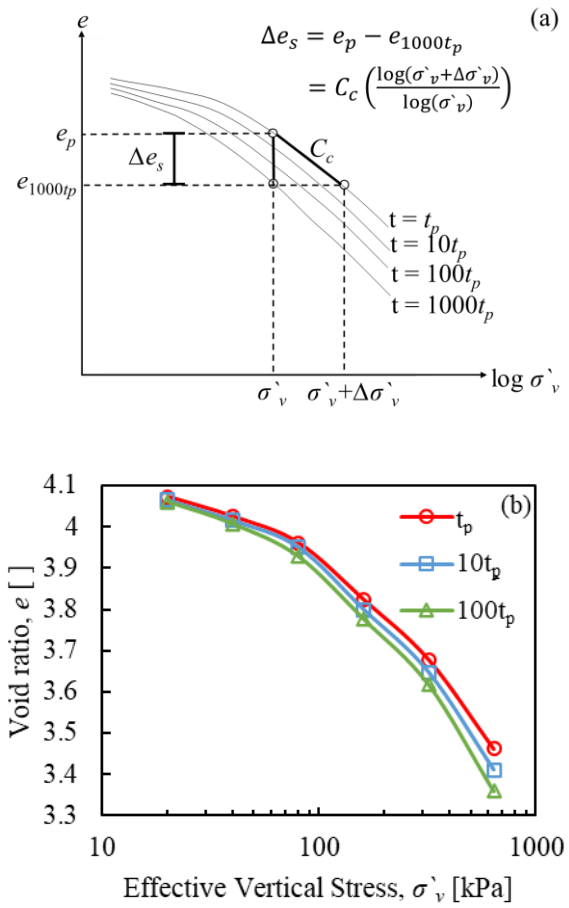

Fig. 10 Secondary compression of biogenic silty soils by the C_α/C_c ratio: (a) The prediction to void ratio change due to the secondary compression (Mesri *et al*. 1997) and (b) Predicted secondary compression of diatomaceous earth

earth content increases, the main matrix of sand-diatomaceous mixtures involves more diatomaceous earth particles and induces plastic deformation due to particle crushing. The presence of diatomaceous earth particles in the soil requires careful consideration during the engineering design process. Diatomaceous earth in the soil can become the critical factor in its compressional behavior and we may underestimate the settlements by conventional approaches when the diatomaceous content is overlooked.

4.3 Significance on secondary compression

Diatomaceous earth shows higher secondary compression compared to other clastic soils. The effect of secondary compression on the settlement varies from low to extremely high depending on vertical pressure from 10 kPa to 1280 kPa, while the secondary compression effect on the settlement of clastic soils is extremely low to low (Mendoza *et al.* 2022, Mesri 1973). Also, the C_α/C_c ratio of diatomaceous earth is similar to fibrous and amorphous peats while the ratios of the other clastic silty soils are close to those of granular soil or shale (Mendoza et al. 2022). The secondary compression index of diatomaceous earth-kaolinite mixtures increases with higher diatomaceous earth content, and the difference among the secondary compression indices of the mixture becomes greater when the vertical stresses increase (Sonyok and Bandini 2019). Therefore, diatomaceous earth is a key factor in controlling the secondary compression of silty soil.

The C_α/C_c ratio can be used to predict the secondary compression of diatomaceous earth. Since C_α/C_c remains constant, the change of C_α with time proportionally correspond to the change of C_c with vertical stress and the changes in the secondary compression void ratio (Δe_s) reflects the void ratio changes caused by an additional pressure ($\Delta\sigma`_v$) at the end of primary consolidation time ($t_p$) in Fig. 10(a) (Mesri *et al.* 1997). The $\Delta\sigma`_v$ is computed

$$\Delta\sigma`_v = \sigma`_v\left[\left(\frac{t}{t_p}\right)^{\frac{C_\alpha}{C_c}} - 1\right] \tag{11}$$

Fig. 10(b) shows the predicted secondary compression curve of the diatomaceous. We can obtain the secondary compression curve at t=t_p, 10t_p, and 100t_p and calculate the void ratio due to the secondary compression. Given that the soils are under vertical stress load of 320 kPa and the secondary compression is allowed until t = 100t_p, we can get the $\Delta\sigma`_v$ by using Eq. (11) and calculate the Δe_s. Diatomaceous earth exhibits Δe_s = 0.1081 while SP, PC, orthoclase, and albite are 0.0037, 0.0052, 0.0031, and 0.0046 respectively. The settlement due to the secondary compression (S_s) of each soil can be calculated using the following equation

$$S_s = H\left(\frac{\Delta e_s}{1+e_p}\right) \tag{12}$$

where H is the thickness of the soil layer.

The study case highlights the secondary compression of diatomaceous earth, which indicates a long-term settlement risk for structures built on such sediments. When we try to improve soil with a preloading beyond the yield stress and the anticipated structural load, particle breakage occurs and induces more compression. We expect that the other clastic silts would experience this yield stress at much higher stress (Kim *et al*. 2019, Mesri and Vardhanabhuti 2009).

In land reclamation, dredged biogenic soils may have a stress condition by the sedimentation below the yield stress. The biogenic soils experience minimal particle breakage and high void ratio. Consequently, the preloading on the dredged biogenic soil may cause the particle breakage and more settlement. Also, the dredged biogenic soil requires more time to stabilize the ground as the soil experiences reduction in permeability and coefficient of consolidation (Figs. 5(b) and 5(d)).

5. Conclusions

Previous studies show that biogenic soils such as diatomaceous earth share similar size and compressibility behavior with low-plasticity silts, yet their presence in clay mixtures affects compressibility differently. The compressional behavior of diatomaceous earth was

analyzed and compared to other silty soils that have similar properties by conducting conventional one-dimensional consolidation experiments. Particle breakage occurs as the primary mechanism differentiating diatomaceous earth from other silty soils. Diatomaceous earth shows recognizable deviation from the intrinsic compression line (ICL) on the normalized compression curve and different trends of the ICL fitting parameters relevant to coefficient of uniformity (C_u) and initial liquidity index (LI_i). These deviations result from mechanical particle breakage that occurs at the vertical stresses of 160 kPa and above. Below 160 kPa, particle breakage is minimal, and the compressional behavior of diatomaceous earth aligns with that of other clastic silty soils. The experimental results offer insights into the compressional behavior of silty soils without particle breakage. Silty soils show that mechanical effects govern the compressibility mechanism, and the coefficient of consolidation (c_v) goes up when vertical stress increases. In contrast, diatomaceous earth shows relatively gentle slope in c_v and even a downward trend at higher vertical stresses, reflecting significant changes in hydraulic conductivity (k) and minimal variation in the coefficient of volume compressibility (m_v) due to particle breakage. Regarding secondary compression, diatomaceous earth demonstrates markedly higher secondary compression index (C_α) and C_α/C_c ratio and induces greater settlement compared to other clastic silty soils.

The compressibility of diatomaceous earth alters overall soil behavior and would deviate from conventional theories from clastic soils. This deviation occurs due to distinct responses below and above the yield stress, where particle breakage increases compressibility. Yield stress serves as a key design factor, because it marks the evident onset of particle breakage. Over the yield stress, engineers should perceive higher compression by the secondary compression of diatomaceous earth.

Acknowledgments

This work was supported by the National Research Foundation of Korea (NRF) grant funded by the Korean government (MSIT) (No. NRF-2021R1F1A1060406).

References

Al-Shamrani, M.A. (2005), "Applying the hyperbolic method and *Cα/Cc* concept for settlement prediction of complex organic-rich soil formations", *Eng. Geol.*, **77**(1-2), 17-34. https://doi.org/10.1016/j.enggeo.2004.07.004.

Aparna, R.P. and Bindu, J. (2023), "Utilization of waste materials as a substitute for the sand drain in clayey soil", *Int. J. Geo-Eng.*, **14**(1), 2. https://doi.org/10.1186/s40703-022-00180-9.

Asaoka, A. (1978), "Observational procedure of settlement prediction", *Soils Found.*, **18**(4), 87-101. https://doi.org/10.3208/sandf1972.18.4_87.

ASTM (2002), Standard Test Methods for Specific Gravity of Soil Solids by Water Pycnometer, ASTM D814, ASTM; West Conshohocken, PA.

ASTM (2011), Standard practice for classification of the soil for engineering purposes (Unified Soil Classification System), ASTM D2487, ASTM; West Conshohocken, PA.

ASTM (2011), Standard test methods for one-dimensional consolidation properties of the soil using incremental loading, ASTM D2435, ASTM; West Conshohocken: PA.

ASTM (2016). Standard Test Method for Particle-Size Distribution (Gradation) of Fine-Grained Soils Using the Sedimentation (Hydrometer) Analysis, ASTM D7928, ASTM; West Conshohocken: PA.

Bohnhoff, G.L. and Shackelford, C.D. (2014), "Consolidation behavior of polymerized bentonite-amended backfills", *J. Geotech. Geoenviron. Eng.*, **140**(5), 04013055. https://doi.org/10.1061/(ASCE)GT.1943-5606.0001079.

Brydon, J.E. and Patry, L.M. (1961), "Mineralogy of champlain sea sediments and a Rideau clay soil profile", *Can. J. Soil Sci.*, **41**(2), 169-181. https://doi.org/10.4141/cjss61-023.

Burland, J.B. (1990), "On the compressibility and shear strength of natural clays", *Géotechnique*, **40**(3), 329-378. https://doi.org/10.1680/geot.1990.40.3.329.

Caicedo, B., Zuluaga, D. and Slebi, C. (2019), "Effects of micro-features of fossil diatom on the macroscopic behaviour of soils", *Géotechnique Lett.*, **9**(4), 322-327. https://doi.org/10.1680/jgele.18.00204.

Chang, C.S. and Deng, Y. (2020), "Modeling for critical state line of granular soil with evolution of grain size distribution due to particle breakage". *Geosci. Frontiers*, **11**(2), 473-486. https://doi.org/10.1016/j.gsf.2019.06.008.

Chapuis, R.P. and Aubertin, M. (2003), "On the use of the Kozeny Carman equation to predict the hydraulic conductivity of soils", *Can. Geotech. J.*, **40**(3), 616-628. https://doi.org/10.1139/t03-013.

Cho, A., Cheong, D., Kim, J.C., Shin, S., Park, Y.H. and Katsuki, K. (2017), "Delta formation in the Nakdong River, Korea, during the Holocene as inferred from the diatom assemblage", *J. Coast. Res.*, **33**(1), 67-77. https://doi.org/10.2112/JCOASTRES-D-15-00240.1.

Díaz-Rodríguez, J.A. and González-Rodríguez, R. (2013), "Influence of diatom microfossils on soil compressibility", *Proceedings of the 18th International Conference on Soil Mechanics and Geotechnical Engineering*, Paris, France, September.

Georgiannou, V.N., Coop, M.R., Altuhafi, F.N. and Lefas, D.I. (2018), "Compression and strength characteristics of two silts of low and high plasticity", *J. Geotech. Geoenviron. Eng.*, **144**(7), 04018041. https://doi.org/10.1061/(ASCE)GT.1943-5606.0001891.

Hoang, N.Q., Kim, S.Y. and Lee, J.S. (2022), "Compressibility, stiffness and electrical resistivity characteristics of sand–diatom mixtures", *Géotechnique*, **72**(12), 1068-1081. https://doi.org/10.1680/jgeot.20.P.136.

Hyodo, M., Wu, Y., Kajiyama, S., Nakata, Y. and Yoshimoto, N. (2017), "Effect of fines on the compression behaviour of poorly graded silica sand", *Geomech. Eng.*, **12**(1), 127-138. https://doi.org/10.12989/gae.2017.12.1.127.

Jang, J., Cao, S.C., Stern, L.A., Jung, J. and Waite, W.F. (2018), "Impact of pore fluid chemistry on fine-grained sediment fabric and compressibility", *J. Geophys. Res. Solid Earth*, **123**(7), 5495-5514. https://doi.org/10.1029/2018JB015872.

Jang, J. and Marjadi, H.K. (2023), "Compressibility of fine-grained sediments based on pore water salinity changes", *Geomech. Eng.*, **33**(1), 113-120. https://doi.org/10.12989/gae.2023.33.1.113.

Jang, J., Waite, W.F., Stern, L.A. and Lee, J.Y. (2022), "Diatom influence on the production characteristics of hydrate-bearing sediments: Examples from Ulleung Basin, offshore South Korea", *Mar. Petroleum Geol.*, **144**, 105834. https://doi.org/10.1016/j.marpetgeo.2022.105834.

Jang, J., Waite, W.F., Stern, L.A., Collett, T.S. and Kumar, P. (2019), "Physical property characteristics of gas hydrate-

bearing reservoir and associated seal sediments collected during NGHP-02 in the Krishna-Godavari Basin, in the offshore of India", *Mar. Petroleum Geol.*, **108**, 249-271. https://doi.org/10.1016/j.marpetgeo.2018.09.027.

Johnson, A., Roy, I.M., Matthews, G.P. and Patel, D. (2003), "An improved simulation of void structure, water retention and hydraulic conductivity in soil with the Pore-Cor three-dimensional network", *Eur. J. Soil Sci.*, **54**(3), 477-490. https://doi.org/10.1046/j.1365-2389.2003.00504.x.

Karabash, Z. and Cabalar, A.F. (2023), "Shear strength response of clay and sand column with different sand grain shapes", *Geomech. Eng.*, **35**(2), 135-147. https://doi.org/10.12989/gae.2023.35.2.135.

Khraisheh, M.A., Al-Ghouti, M.A., Allen, S.J. and Ahmad, M.N. (2005), "Effect of OH and silanol groups in the removal of dyes from aqueous solution using diatomite", *Water Res.*, **39**(5), 922-932. https://doi.org/10.1016/j.watres.2004.12.008.

Kwon, Y.M., Chang, I., Lee, M. and Cho, G.C. (2019), "Geotechnical engineering behavior of biopolymer-treated soft marine soil", *Geomech. Eng.*, **17**(5), 453-464. https://doi.org/10.12989/gae.2019.17.5.453.

Kim, J., Dai, S., Jang, J., Waite, W.F., Collett, T.S. and Kumar, P. (2019), "Compressibility and particle crushing of Krishna-Godavari Basin sediments from offshore India: Implications for gas production from deep-water gas hydrate deposits", *Mar. Petroleum Geol.*, **108**, 697-704. https://doi.org/10.1016/j.marpetgeo.2018.07.012.

Lambe, T.W. and Whitman, R.V. (1969), *Soil mechanics*. John Wiley & Sons, New York, USA.

Li, C. (2014), "A simplified method for prediction of embankment settlement in clays", *J. Rock Mech. Geotech. Eng.*, **6**(1), 61-66. https://doi.org/10.1016/j.jrmge.2013.12.002.

Li, P.P., Li, J.P., Liu, G.Y. and Zhou, P. (2024), "Prediction of dredged soil settlement based on improved BP neural network", *Proceedings of the IOP Conference Series: Earth and Environmental Science*, **1337**(1), 012013.

Li, S., Huang, M., Cui, M., Lin, P., Xu, L. and Xu, K. (2023), "Stabilization of cement-soil utilizing microbially induced carbonate precipitation", *Geomech. Eng.*, **35**(1), 95-108. https://doi.org/10.12989/gae.2023.35.1.095.

Li, X., Liu, Y., Qian, G., Liu, X., Wang, H. and Yin, G. (2023), "Numerical investigation into particle crushing effects on the shear behavior of gravel", *Geomech. Eng.*, **35**(2), 209-219. https://doi.org/10.12989/gae.2023.35.2.209.

Mendoza, C., Caicedo, B. and Duque, J. (2022). "Technical report on the compression, structure, and creep behaviors of lacustrine soil deposits in Bogotá, Colombia", *Soils Found.*, **62**(5), 101215. https://doi.org/10.1016/j.sandf.2022.101215.

Mesri, G. (1973), "Coefficient of secondary compression", *J. Soil Mech. Found. Division*, **99**(1), 123-137. https://doi.org/10.1061/JSFEAQ.0001840.

Mesri, G. and Castro, A. (1987), "C_α/C_c concept and K_0 during secondary compression", *J. Geotech. Eng.*, **113**(3), 230-247. https://doi.org/10.1061/(ASCE)0733-9410(1987)113:3(230).

Mesri, G., Stark, T.D., Ajlouni, M.A. and Chen, C.S. (1997), "Secondary compression of peat with or without surcharging", *J. Geotech. Geoenviron. Eng.*, **123**(5), 411-421. https://doi.org/10.1061/(ASCE)1090-0241(1997)123:5(411).

Mesri, G. and Godlewski, P.M. (1977), "Time-and stress-compressibility interrelationship", *J. Geotech. Eng. Division*, **103**(5), 417-430. https://doi.org/10.1061/AJGEB6.0000421.

Mesri, G. and Vardhanabhuti, B. (2009), "Compression of granular materials", *Can. Geotech. J.*, **46**(4), 369-392. https://doi.org/10.1139/T08-123.

Minh, N.H. and Cheng, Y.P. (2013), "A DEM investigation of the effect of particle-size distribution on one-dimensional compression", *Géotechnique*, **63**(1), 44-53. https://doi.org/10.1680/geot.10.P.058.

Ng, C.W., Liu, G.B. and Li, Q. (2013), "Investigation of the long-term tunnel settlement mechanisms of the first metro line in Shanghai", *Can. Geotech. J.*, **50**(6), 674-684. https://doi.org/10.1139/cgj-2012-0298.

Nguyen, A.D., Nguyen, V.T. and Kim, Y.S. (2023), "Finite element analysis on dynamic behavior of sheet pile quay wall dredged and improved seaside subsoil using cement deep mixing", *Int. J. Geo-Eng.*, **14**(1), 9. https://doi.org/10.1186/s40703-023-00186-x.

Nichols, G. (2009), *Sedimentology and Stratigraphy*, John Wiley & Sons, New York, USA.

Pedone, A., Malavasi, G., Menziani, M.C., Segre, U. and Cormack, A.N. (2008), "Molecular dynamics studies of stress− strain behavior of silica glass under a tensile load", *Chem. Mater.*, **20**(13), 4356-4366. https://doi.org/10.1021/cm800413v.

Perisic, G.A., Ovalle, C. and Barrios, A. (2019), "Compressibility and creep of a diatomaceous soil", *Eng. Geol.*, **258**, 105145. https://doi.org/10.1016/j.enggeo.2019.105145.

Robinson, R.G. and Allam, M.M. (1998). "Effect of clay mineralogy on coefficient of consolidation", *Clays and Clay Minerals*, **46**(5), 596-600. https://doi.org/10.1346/CCMN.1998.0460514.

Santamarina, J.C., Klein, A. and Fam, M.A. (2001), *Soils and waves: Particulate Materials Behavior, Characterization and Process Monitoring*. John Wiley, New York, USA.

Santamarina, J.C., Klein, K.A., Wang, Y.H. and Prencke, E. (2002), "Specific surface: Determination and relevance", *Can. Geotech. J.*, **39**(1), 233-241. https://doi.org/10.1139/t01-077.

Scarciglia, F., Pulice, I., Robustelli, G. and Vecchio, G. (2006). "Soil chronosequences on Quaternary marine terraces along the northwestern coast of Calabria (Southern Italy)", *Quaternary Int.*, **156**, 133-155. https://doi.org/10.1016/j.quaint.2006.05.027.

Shiwakoti, D.R., Tanaka, H., Tanaka, M. and Locat, J. (2002), "Influences of diatom microfossils on engineering properties of soils", *Soils Found.*, **42**(3), 1-17. https://doi.org/10.3208/sandf.42.3_1.

Sobhan, K., Ramirez, J.C. and Reddy, D.V. (2012), "Cement stabilization of highly organic subgrade soils to control secondary compression settlement", *Transport. Res. Record*, **2310**(1), 103-112. https://doi.org/10.3141/2310-11.

Sonyok, D.R. and Bandini, P. (2019), "Oedometric behavior of Diatomite–Kaolin mixtures", *J. Geotech. Geoenviron. Eng.*, **145**(9), 06019005. https://doi.org/10.1061/(ASCE)GT.1943-5606.0002084.

Sridharan, A. and Rao, A.S. (1981), "Rectangular hyperbola fitting method for one dimensional consolidation", *Geotech. Test. J.*, **4**(4), 161-168. https://doi.org/10.1520/GTJ10785J.

Stark, T.D., Choi, H. and Schroeder, P.R. (2005), "Settlement of dredged and contaminated material placement areas. I: Theory and use of primary consolidation, secondary compression, and desiccation of dredged fill", *J. Waterway, Port, Coast. Ocean Eng.*, **131**(2), 43-51. https://doi.org/10.1061/(ASCE)0733-950X(2005)131:2(43).

Tan, S. and Chew, S. (1996), "Comparison of the hyperbolic and Asaoka observational method of monitoring consolidation with vertical drains", *Soils Found.*, **36**(3), 31-42. https://doi.org/10.3208/sandf.36.3_31.

Taylor, D.W. (1948), *Fundamentals of Soil Mechanics*. Wiley, New York, USA.

Tiwari, B. and Ajmera, B. (2011), "A new correlation relating the shear strength of reconstituted soil to the proportions of clay minerals and plasticity characteristics", *Appl. Clay Sci.*, **53**(1), 48-57. https://doi.org/10.1016/j.clay.2011.04.021.

Tiwari, B. and Ajmera, B. (2012), "New correlation equations for compression index of remolded clays", *J. Geotech. Geoenviron. Eng.*, **138**(6), 757-762.

https://doi.org/10.1061/(ASCE)GT.1943-5606.0000639.
Wang, Y., Wei, T., Ren, Y., Gao, Y. and Yang, Q. (2022), "Experiment study on normalized compression behaviour of marine diatomaceous soil considering microstructure of biogenic silica", *Appl. Ocean Res.*, **125**, 103254. https://doi.org/10.1016/j.apor.2022.103254.
Xiao, Y., Liu, H., Chen, Q., Ma, Q., Xiang, Y. and Zheng, Y. (2017), "Particle breakage and deformation of carbonate sands with wide range of densities during compression loading process", *Acta Geotechnica*, **12**, 1177-1184. https://doi.org/10.1007/s11440-017-0580-y.
Zhang, Q., Li, S., Liang, F., Yang, M. and Zhang, Q. (2014), "Simplified method for settlement prediction of single pile and pile group using a hyperbolic model", *Int. J. Civil Eng*., **12**(2), 146-157.
Zuluaga-Astudillo, D., Ruge, J.C., Camacho-Tauta, J., Reyes-Ortiz, O. and Caicedo-Hormaza, B. (2022), "Diatomaceous soils and advances in geotechnical engineering—Part I", *Appl. Sci.*, **13**(1), 549. https://doi.org/10.3390/app13010549.